RSC Advances

RSC Publishing

PAPER

View Article Online
View Journal | View Issue

Rational design of a high performance all solid state flexible micro-supercapacitor on paper†

Cite this: *RSC Advances*, 2013, **3**, 15827

Xu Wang,[a] Afriyanti Sumboja,[a] Wan Ling Foo,[a] Chao Yi Yan,[a] Kazuhito Tsukagoshi*[bc] and Pooi See Lee*[a]

Received 16th April 2013,
Accepted 28th June 2013

DOI: 10.1039/c3ra41807c

www.rsc.org/advances

Micro-supercapacitors have attracted considerable attention due to their feasibility as power supplies for future integration into autonomous and portable devices. However, the conventional lab-on-chip fabrication method requires multiple patterning and metallization procedures, while the rigid substrate restricts versatility in applications such as flexible and wearable electronics. Here, we report the low cost, facile and scalable fabrication process of an all solid state flexible micro-supercapacitor on commercially available photo paper for the first time. Three dimensional interconnected coral-like polyaniline–manganese oxide composite material is electrochemically deposited on the interdigital finger electrodes. Electrochemical measurements reveal that the high aspect ratio finger electrode pattern and small gap interdigital finger electrode design is crucial to ensure superior performance. The optimized device shows an ultra high areal energy density of 6.3 μW h cm^{-2} at a power density of 35 μW cm^{-2} (94.73 mF cm^{-2} at 0.1 mA cm^{-2}), while it maintains 4.8 μW h cm^{-2} at a power density of 3500 μW cm^{-2} (71.43 mF cm^{-2} at 10.0 mA cm^{-2}). Meanwhile, it also has good flexibility. Such a flexible micro-supercapacitor is promising for future applications in lightweight, wearable or foldable electronics.

Introduction

Recent trends in developing functional miniaturized/portable electronic devices, such as autonomous devices,[1] flexible/wearable electronics[2,3] and active artificial skins,[4,5] require a high performance, compact, light weight and integrable energy storage/supply module to ensure functionality. Micro-supercapacitors, which have an in-plane interdigital finger electrode design with micro scale gaps, are attracting increasing attention.[6–8] Such a design is believed to efficiently minimize the overall area and thickness and maximize the electrode utilization for the power sources.[6,9,10] Meanwhile, compared to other energy storage devices, such as micro-batteries, micro-supercapacitors are not expected to experience a dramatic reduction in performance in the micro-scale architecture.[11] Nearly all the efforts to date have focused on the fabrication of micro-supercapacitors on rigid SiO_2–Si substrates. The interdigital finger electrode pattern can be fabricated through consecutive patterning and metallization processes. Nevertheless, the silicon wafer based process limits the possibility of future flexible/wearable electronics applications. Apart from device processing, the electrode material selection in current micro-supercapacitors focuses mainly on carbon materials, which usually have low energy density[6,7,9] and trade off the advantage of the small area of the micro-supercapacitor. Pseudocapacitive materials, which store energy through faradic redox reactions, are promising to elevate the energy density. MnO_2,[12] polypyrrole,[13] and polyaniline[8] have been investigated as electrode materials in a limited number of reports for micro-supercapacitors. However, previous workers have encountered different problems, such as poor rate performance,[12] poor stability[13] and low areal energy density.[8,12,13] Thus, the development of a flexible micro-supercapacitor with high performance is of great importance in meeting the requirements of future applications in flexible/wearable electronics.

Paper is a traditional fibrous material which was invented thousands of years ago. This low cost, flexible and environmentally friendly material may be the ideal substrate for the development of a flexible micro-supercapacitor. However, the high surface roughness of paper is a major concern for metallic interconnections and functional device fabrication.[14] This makes future integration of functional electronic counter-

[a]*School of Materials Science and Engineering, Nanyang Technological University, 639798, Singapore. E-mail: pslee@ntu.edu.sg*
[b]*International Center for Materials Nanoarchitectonics (WPI-MANA), National Institute for Materials Science, Tsukuba, Ibaraki 305–0044, Japan. E-mail: TSUKAGOSHI.Kazuhito@nims.go.jp*
[c]*CREST, JST, Kawaguchi, Saitama 305–0044, Japan*

† Electronic supplementary information (ESI) available: Schematic illustration of the micro-supercapacitor device fabrication process; optical microscopy images of Au electrode patterns; specifics of interdigital finger electrode pattern designs; SEM images of pure PANI electrochemically deposited on Au electrode patterns; working potential optimization of the micro-supercapacitor device; Nyquist plots of sample MC-5-200 tested in aqueous and gel electrolytes; electrochemical tests for the pure PANI micro-supercapacitor device; digital images of device flexibility. See DOI: 10.1039/c3ra41807c

parts on paper substrates difficult. As a result, the reports of paper substrate based energy storage devices are still scarce. Parylene is a commercially available polymer, which is widely used for insulation and moisture/chemical resistant coatings.[14,15] Meanwhile, it is also demonstrated that parylene is helpful in reducing the surface roughness of paper substrates.[14] On the other hand, in terms of electrode material selection, conducting polymer–metal oxide composite materials are attracting extensive attention in conventional supercapacitor research due to the merits of enhanced electric conductivity as well as additional faradic reactions brought about by the conducting polymer content.[16–18] It is therefore a great option for overcoming the problems encountered in current pseudocapacitive material based micro-supercapacitor research.

Here, we present the first report of the design and fabrication of a high performance all solid state flexible micro-supercapacitor on parylene passivated paper. Three dimensional interconnected polyaniline–manganese oxide composite materials are electrochemically deposited on interdigital finger electrodes. High aspect ratio and small inter-electrode gap design is found to be crucial in improving the overall device performance. The optimized device shows an ultra high areal energy density of 6.3 μW h cm^{-2} at a power density of 35 μW cm^{-2} (94.73 mF cm^{-2} at 0.1 mA cm^{-2}), while it maintains 4.8 μW h cm^{-2} at a power density of 3500 μW cm^{-2} (71.43 mF cm^{-2} at 10.0 mA cm^{-2}). Such values are the best for micro-supercapacitors reported to date. With an appropriate hard mask design, it is feasible to print micro-supercapacitor units reproducibly on a large scale. It also makes future integration with functional electronics units on paper possible. This micro-supercapacitor on parylene–paper makes significant advances towards future scalable and high performance energy storage applications in flexible/wearable electronics.

Experimental

Fabrication of interdigital finger electrodes on paper

The fabrication process for the micro-supercapacitor on paper is presented in the ESI.† Briefly, commercially available photographic paper (purchased from Canon Co.) was cut into 1.5 cm × 1.5 cm pieces and was used without any cleaning procedures. Parylene was then thermally evaporated onto the paper for waterproofing and insulation purposes. 200 nm gold patterns were then directly thermally evaporated onto the parylene passivated paper using different hard masks. The specific parameters (length and width) of the gold electrodes matched well with the design of the hard masks. Optical images of the interdigital finger electrodes are shown in Fig. S1, ESI† and the specifics of the electrode patterns are listed in Table S1, ESI.† The electrode patterns are labelled as sample MC-1, MC-2, MC-3, MC-4, MC-5 and MC-6.

Electrochemical deposition of polyaniline–manganese oxide composite material

Polyaniline–manganese oxide (PANI–MnO_x) was electrochemically deposited onto the gold electrode in a three electrode cell using Ag/AgCl as the reference electrode and Pt as the counter electrode. Potentially dynamic deposition (cyclic voltammetry (CV) deposition) was carried out in a mixed solution of 0.1 M aniline, 0.12 M manganese acetate and 0.5 M sulfuric acid using a scan rate of 0.2 V s^{-1} from −0.2 to 0.9 V with an appropriate number of cycles.

Structural characterization

The structures of the products were characterized using scanning electron microscopy (FESEM; JEOL, JSM-7600F), transmission electron microscopy (TEM; JEOL, JEM-2100), electron dispersive X-ray spectroscopy (EDX) and X-ray photoelectron spectroscopy (XPS).

Preparation of the poly(vinyl alcohol)–phosphoric acid (PVA–H_3PO_4) gel electrolyte

Briefly, 6 g PVA and 6 g H_3PO_4 were added into 60 ml DI water and were vigorously stirred at 85 °C until complete dissolution was achieved.

Electrochemical tests

For the purpose of optimizing the interdigital finger electrode design, 1 M H_2SO_4 was used as the electrolyte for all the electrochemical tests. After device structure and electrochemical deposition optimization, all the electrochemical tests were carried out using the PVA–H_3PO_4 gel electrolyte.

Results and discussion

Structural characterization

The fabricated electrode patterns are labelled as MC-1, MC-2, MC-3, MC-4, MC-5, and MC-6, with the specifics shown in Table S1, ESI.† The electrochemically deposited PANI–MnO_x composite materials on different interdigital finger electrodes all show similar morphologies. Typical morphologies of a sample on MC-6, prepared with 150 CV cycles (sample MC-6-150) are shown in Fig. 1. As shown in Fig. 1a, under low magnification SEM, the Au electrodes are fully covered with fluffy material, while a clean area is observed in the electrode gaps. Closer examination in Fig. 1b–d shows that the electrode material has a three dimensional interconnected porous structure which resembles the structure of coral. This composite material consists of dendritic PANI–MnO_x structures with random branches. The diameter of individual dendrite is over 100 nm. Coral like porous structures will be more accessible to the electrolyte and will be more beneficial for electrolyte diffusion and material utilization. Meanwhile, the highly conductive PANI–MnO_x matrix is also beneficial for electron conduction. In contrast, the absence of Mn^{2+} in the deposition precursor results in a dense PANI film with a much less open structure, which is not favourable for fast electrolyte diffusion.

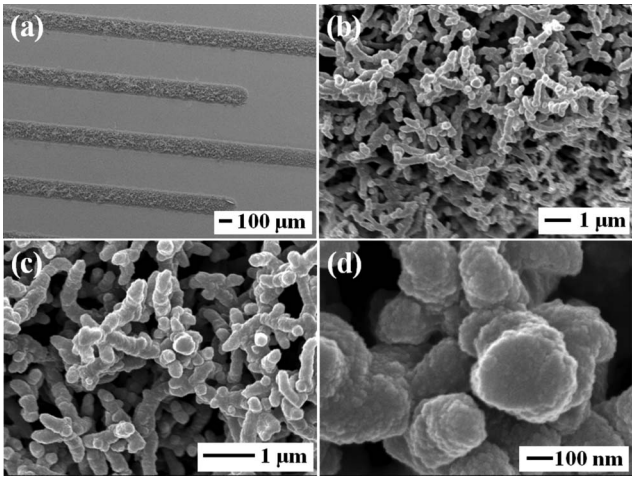

Fig. 1 SEM images of PANI–MnO_x composite material on interdigital finger electrodes, sample MC-6-150.

To provide further information about the structure of the composite material, a TEM image is shown in Fig. 2a. Echoing the observation in the SEM image in Fig. 1, the composite material also shows an interconnected dendritic structure under TEM. The chemical composition of the composite material was determined by TEM based EDX. The Mn comes from the MnO_x in the composite material, while S originates from the sulfate anions doped in the PANI.[19] C comes from both the PANI and the TEM grid. The Cu signal comes from the TEM grid and the Si is from the TEM background signal, which is also detected at a sample free location. To elucidate the crystallinity of the composite material, selected area electron diffraction (SAED) was performed on the area shown in Fig. 2c. As shown in Fig. 2d, there is no diffraction ring detected, which suggests that the PANI–MnO_x composite material is amorphous.

Detailed investigation of the element chemical states in the amorphous PANI–MnO_x composite material was carried out using XPS. Deconvolution of the C 1s core-level spectrum results in three peaks correlated to three different electronic states as shown in Fig. 3a. The C=C (284.7 eV) and C–N (286.3 eV) peaks are from PANI,[20] while the C–O bonds (288.3 eV) may come from impurities in the aniline monomer. The deconvolution of the N 1s spectrum in Fig. 3b shows three peaks from the cationic nitrogen radical (N^+) at 401.9 eV, the benzenoid amine (–NH–) at 399.7 eV and the quinoid amine (–N=) at 398.3 eV, which match well with previous reports.[20–22] It was found that the PANI–MnO_x composite material consists mainly of cationic nitrogen radicals and benzenoid amines, which indicates a high doping level of PANI and ensures a good electronic conductivity.[23] The binding energy of Mn $2p_{3/2}$ is 641.9 eV as shown in Fig. 3c, which is between that of Mn^{3+} and Mn^{4+}.[24] Thus, we suggest that the PANI–MnO_x composite material consists of highly doped PANI and mixed manganese oxide with both +3 and +4 oxidation states. Meanwhile, the atomic ratio of Mn/N is 1 : 15, as calculated from the XPS study.

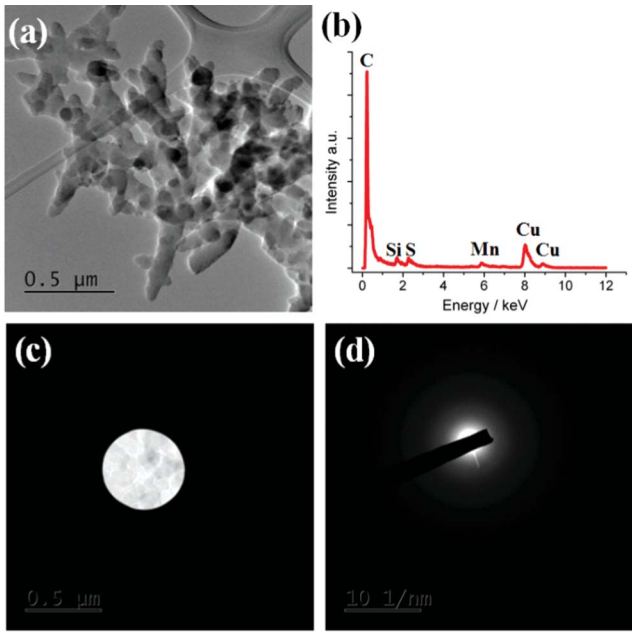

Fig. 2 (a) TEM image of PANI–MnO_x composite material, sample MC-6-150; (b) EDX spectrum of PANI–MnO_x composite material, sample MC-6-150; (c) TEM image of SAED area; (d) SAED image of PANI–MnO_x composite material.

Electrochemical characterization

Influence of interdigital finger electrode design on electrochemical performance

Despite the previous reports on micro-supercapacitors, the influence of interdigital finger electrode design on device performance is seldom addressed specifically.[6,7] Here, we first investigate the optimum design of the aspect ratio of the interdigital finger electrode and the inter-electrode gap

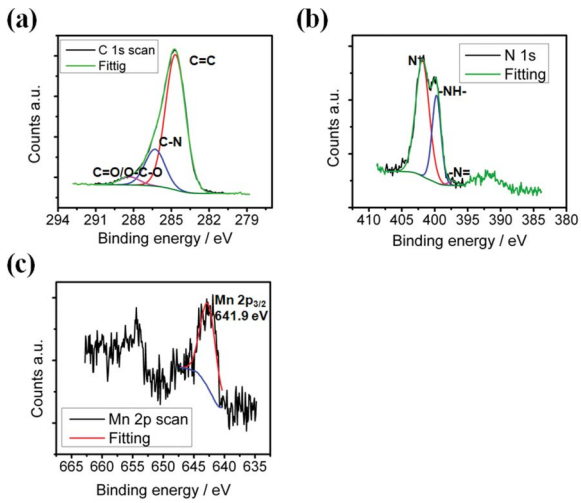

Fig. 3 (a) C 1s scan and fitting of the PANI–MnO_x composite material; (b) N 1s scan and fitting of the PANI–MnO_x composite material; (c) Mn 2p scan and fitting of PANI–MnO_x composite material.

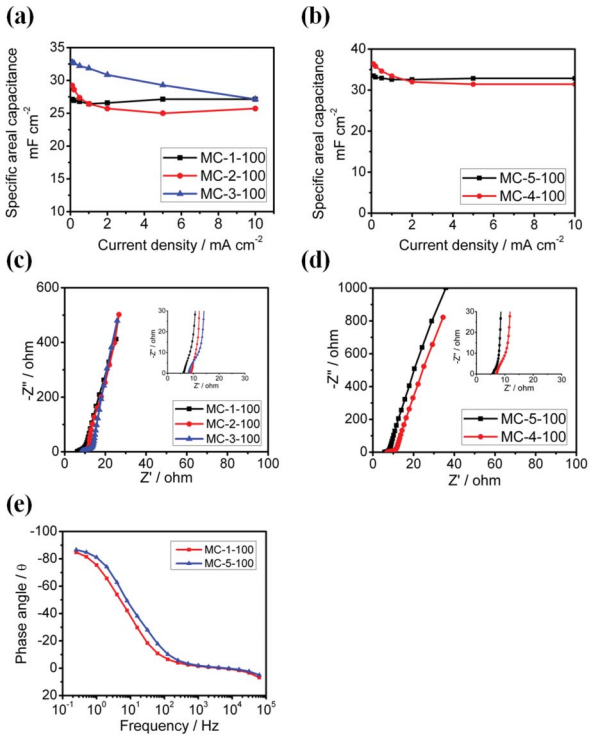

Fig. 4 (a) Relationship between specific areal capacitance and current density for samples MC-1-100, MC-2-100 and MC-3-100; (b) relationship between specific areal capacitance and current density for sample MC-4-100, MC-5-100; (c) Nyquist plots for samples MC-1-100, MC-2-100 and MC-3-100; (d) Nyquist plots for sample MC-4-100 and MC-5-100; (e) Bode plots for samples MC-1-100 and MC-5-100.

distance before further electrochemical deposition optimization. Micro-electrode patterns MC-1, MC-2 and MC-3 (refer to Table S1, ESI)† were deposited with PANI–MnO_x from −0.2 V–0.9 V for 100 cycles, and the samples after deposition were labelled as sample MC-1-100, MC-2-100, and MC-3-100 respectively. The optimum operation window for the symmetric devices was determined to be 0–0.7 V as shown in Fig. S3, ESI.† The higher operation window shows distinct distortion of CV curves and a decrease in coulombic efficiency as shown in Fig. S3a and b, ESI† respectively. The specific areal capacitances (C_{area}) of sample MC-1-100, MC-2-100 and MC-3-100 at various current densities were determined using a galvanostatic charge–discharge test and are shown in Fig. 4a. The discharge capacitance can be calculated from the discharge curve after *IR* drop as in eqn (1).

$$C_{area} = I\Delta t/A\Delta V \quad (1)$$

Where I is the current, Δt is the discharge time after *IR* drop, A is the total area of the interdigital finger electrode array and ΔV is the potential window of the symmetric capacitor. Sample MC-3-100 shows the highest C_{area} = 32.79 mF cm^{-2} at 0.1 mA cm^{-2} with 82.9% retention of capacity at 10 mA cm^{-2}. Sample MC-1-100 shows virtually no degradation of capacity at high current density. Such high rate performance for the micro-supercapacitor is due to the short diffusion paths used in the interdigital finger electrode design.[6–8] As the total areal and electrode gap of pattern MC-1, MC-2 and MC-3 are the same, the increase of C_{area} may be due to the difference in the deposited active material masses caused by the different aspect ratios of individual finger electrodes.

It is widely accepted that during electrochemical experiments, the electrode geometry will influence the flux of mass diffusion of the electrolyte.[25–27] Our results suggest that the different designs of finger electrodes would vary mass diffusion around the patterned gold electrodes during electrochemical deposition. The high aspect ratio interdigital finger electrodes with higher pattern density lead to a higher mass loading under the same electrochemical deposition conditions.

To further elucidate the electrochemical behavior caused by electrode design, the electrochemical impedance (EIS) studies of samples MC-1-100, MC-2-100 and MC-3-100 were carried out as shown in Fig. 4c. In Fig. 4c, it is clearly shown that sample MC-1-100 has the smallest intercept with the x axis (∼6.1 Ω), which means it has the lowest equivalent series resistance (ESR) among all three samples.[28] It is also noteworthy to mention that, this ESR value is much lower than the ESR values reported in pseudocapacitive material based micro-supercapacitors.[8] The difference in ESR may be attributed to the increase in ohmic resistance induced by the decrease in electrode width ($R = \rho l/A$). Thus, sample MC-1-100 presents the best rate performance (Fig. 4a). On the other hand, all samples show nearly 90° linear curves at low frequency regions, which indicate ideal capacitor behavior.[29,30] Considering both specific areal capacitance and rate performance, we decided to use the 100 μm electrode width for further structural optimization.

Interdigital electrode patterns MC-4 (500 μm gap), MC-5 (300 μm gap) and MC-6 (100 μm gap) with 100 μm electrode widths were used for electrochemical deposition under the same conditions described above. The samples were labelled as MC-4-100, MC-5-100 and MC-6-100. The sample MC-6-100 showed a short circuit for the two electrode test, which indicates a connection between two adjacent electrodes. It also suggests that the mass diffusion during deposition is influenced by the geometry design of the interdigital finger electrodes. Samples MC-4-100 and MC-5-100 worked well and the electrochemical performances are shown in Fig. 4b. At 0.1 mA cm^{-2}, MC-4-100 and MC-5-100 present specific areal capacitances of 36.4 mF cm^{-2} and 33.5 mF cm^{-2}, respectively, while sample MC-5-100 shows much better rate performance. As shown in Fig. 4d, sample MC-4-100 shows a more obvious 45° Warburg resistance curve compared with sample MC-5-100.[31,32] The improved rate performance is realized by the reduced electrode gap in pattern MC-5. The smaller electrode gap leads to a shortened diffusion length for the electrolyte ions. It facilitates electrolyte diffusion during the electrochemical test.

For a more informative analysis of EIS, Bode plots of samples MC-1-100 and MC-5-100 are shown in Fig. 4e. The frequency response of a supercapacitor can be compared using the characteristic frequency f_0 where the frequency corresponds to the phase angle at −45°.[7,33] The characteristic frequency marks the point at which the resistive and capacitive

impedances are equal and at frequencies higher than f_0 the supercapacitor shows more resistive behavior.[7,33] The corresponding relaxation time constant ($\tau_0 = 1/f_0$) is the minimum time needed to discharge all the energy from the device with an efficiency of greater than 50%. As shown in Fig. 4e, sample MC-5-100 (f_0 = 10.16 Hz, τ_0 = 98 ms) shows the better frequency response compared to sample MC-1-100 (f_0 = 6.46 Hz, τ_0 = 154.7 ms). This indicates a better frequency response for the micro-supercapacitor can be achieved by using a high aspect ratio and small inter-electrode gap design.

In summary, the optimum strategy for interdigital electrode design for micro-supercapacitors is to fabricate high aspect ratio electrodes with small inter-electrode gaps. A 300 μm electrode gap with 100 μm electrode width (pattern MC-5) is the optimum electrode design for PANI–MnO_x composite material micro-supercapacitors. Such a design is able to ensure a high specific areal capacitance, high rate performance as well as a high frequency response.

High performance flexible PANI–MnO_x symmetric supercapacitor

Knowing the optimum interdigital finger electrode design, the electrochemical deposition was further optimized based on pattern MC-5. It was found that 200 cycles of CV deposition showed the best specific areal capacitance. The sample was labelled as MC-5-200 and it was tested in PVA–H_3PO_4 gel electrolyte. The corresponding electrochemical test results are shown in Fig. 5. As shown in Fig. 5a, the CV curves of sample MC-5-200 show typical rectangular shapes at different scan rates, which indicates typical capacitor performance with good rate capability.[32] In Fig. 5b, the charge–discharge curves of sample MC-5-200 all show symmetric triangular shapes indicating good capacitor behaviour.[28,34] The specific areal capacitances calculated from the charge–discharge tests are

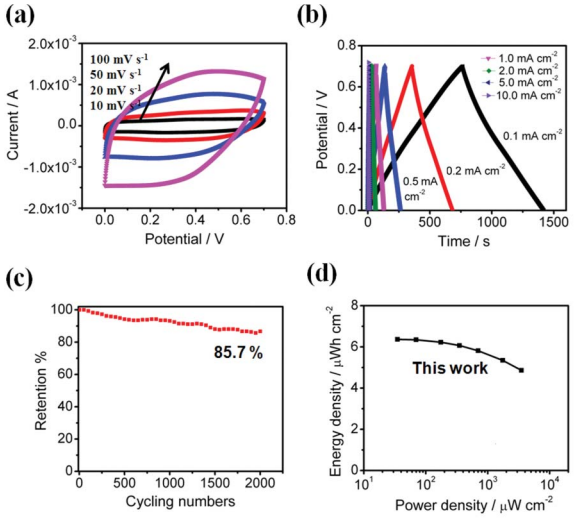

Fig. 5 (a) CV curves of sample MC-5-200 tested in gel electrolyte at different scan rates; (b) charge–discharge curves of sample MC-5-200 tested in gel electrolyte at different current densities; (c) cycling test of sample MC-5-200 tested at 0.5 mA cm^{-2} in gel electrolyte; (d) Ragone plot of sample MC-5-200 in gel electrolyte.

94.73 mF cm^{-2} at 0.1 mA cm^{-2}, and it remained as high as 71.43 mF cm^{-2} at 1.0 mA cm^{-2} (73.1% retention). The capacitance loss at high current density is much higher than when testing in aqueous electrolyte. This may be due to the slower ion diffusion in gel electrolyte as demonstrated in Fig. S4, ESI.† As shown in the Nyquist plots, sample tested in gel electrolyte shows obvious Warburg resistance in the high frequency region.[28,29]

Despite the relatively slow electrolyte diffusion in the gel electrolyte, the devices still present a high areal capacitance compared with previous reports.[8] We further highlight the importance of MnO_x in enhancing the areal capacitance of the micro-supercapacitor devices. As shown in Fig. S5, ESI,† the symmetric device using PANI only has a specific areal capacitance of 34.1 mF cm^{-2}, which is 36% of that of the composite electrode material. The pseudocapacitive behaviors of both MnO_x and PANI within the same potential window ensure the elevated areal capacitance of the symmetric device.[17,35]

Prolonged cycling is another important parameter in practical applications. The cycling test for our device was performed at a charge–discharge current density of 0.5 mA cm^{-2}, as shown in Fig. 5c. The sample MC-5-200 only experiences 14.3% capacitance loss after 2000 cycles, showing a good cycling stability. These energy and power characteristics are crucial for energy storage devices. To demonstrate the operation characteristics of our asymmetric supercapacitor device, the relationship between the energy densities and the average power densities according to CV tests was calculated based on eqn (2) and (3):[31,36]

$$E_{area} = C_{area}V^2/2 \quad (2)$$

$$P_{area} = E_{area}/t \quad (3)$$

where C_{area} is the specific areal capacitance calculated from the charge–discharge test, V is the working potential and t is the discharge time. The Ragone plot of sample MC-5-200 is shown in Fig. 5d. Our device shows a high energy density, 6.3 μW h cm^{-2} at a power density of 35 μW cm^{-2}, while it maintains 4.8 μW h cm^{-2} at a power density of 3500 μW cm^{-2}. Our device is therefore suitable for high energy and power storage delivery in microscale systems, such as active radio-frequency identification (RFID) tags, wireless sensors and self-powered devices.

To demonstrate the flexibility of paper based micro-supercapacitors, sample MC-5-200 was bent over different rigid supports with various diameters. A quartz tube with a diameter of 1.5 cm is shown in Fig. S6a, ESI† as an example. The extent of device bending can be described by the radius of each rigid support. The electrochemical tests were carried out and the results are shown in Fig. 6. As shown in Fig. 6a, the CV curves for sample MC-5-200 all exhibited well defined rectangular shapes in both normal and bent states, indicating negligible influence of bending on the supercapacitor behaviour. However, the areas of the CV curves in the bent states are slightly smaller than those in the normal state, which suggests slight capacitance reduction in bent states. The specific

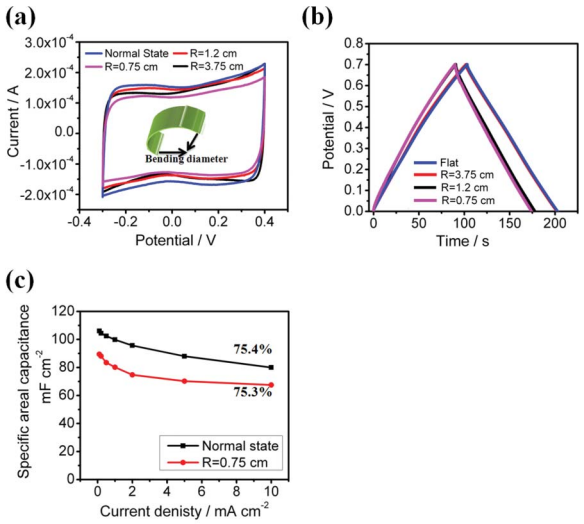

Fig. 6 (a) CV curves of sample MC-5-200 in normal and bent states at a scan rate of 10 mV s^{-1} (inset is an illustration of the bending test); (b) charge–discharge curves of MC-5-200 in normal and bent states at a current density of 1.0 mA cm^{-2}; (c) relationship between specific areal capacitance and current density for a sample of MC-5-200 in normal and bent states, R = 0.75 cm, the percentage indicates the capacitance retention.

capacitances in the bent states were calculated from charge–discharge tests as shown in Fig. 6b and c. In Fig. 6b, the capacitance in the bent state R = 0.75 cm is 84.7% that of the normal state, while the capacitance maintains 87.1% and 96.7% for the bent states R = 1.2 cm and 3.75 cm respectively. The bending may cause mechanical strain on the electrodes and materials as well as on the gel electrolyte. In Fig. 6c, the very similar rate capabilities for the flat and bent state (R = 0.75 cm) suggest that the fast electrochemical reaction and electrolyte diffusion are not significantly affected by bending. These results clearly prove good flexibility of our paper based micro-supercapacitor. A wearable paper based device on a bent wrist is demonstrated in Fig. S6b, ESI.†

The outstanding electrochemical performance of this flexible PANI–MnO_x symmetric micro-supercapacitor can be attributed to the following few points: 1) the paper substrate is naturally flexible; 2) the in plane micro-supercapacitor design ensures good mechanical properties by eliminating the conventional sandwich device structure; 3) the interdigital finger electrode design ensures fast electrolyte diffusion and provides a high rate performance; 4) the 3D interconnected PANI–MnO_x coral like electrode material ensures high electrochemical energy storage. First of all the pseudocapacitive response of MnO_x and PANI fall in the same potential range, which is around 0–0.8 V *vs.* Ag/AgCl reference electrode. In this sense, the oxidation and reduction of both PANI and MnO_x occur almost at the same time. As both PANI and MnO_x have consecutive oxidation/reduction states within the whole range, the charge storage ability will be greatly enhanced compared with either single component. Secondly, in our case, the conductive PANI surrounding MnO_x leads to fast electron transportation. Thirdly, the highly macroporous structure ensures fast electrolyte transfer within the material matrix. Thus, there is an elevation in the overall material performance. Thus, this flexible PANI–MnO_x micro-supercapacitor on paper is promising for future flexible and wearable electronics applications.

Conclusion

A flexible micro-supercapacitor was successfully fabricated using 3D PANI–MnO_x as an electrode material on a parylene passivated paper substrate. Based on in-depth electrochemical studies, we suggest that high aspect ratio interdigital finger electrodes with small inter-electrode gaps is a favourable design for high performance micro-supercapacitor. Based on the optimum design, the symmetric device is able to achieve a high energy density of 6.3 μW h cm^{-2} at a power density of 35 μW cm^{-2}, while it maintains 4.8 μW h cm^{-2} at a power density of 3500 μW cm^{-2}. The excellent flexibility of our device is demonstrated as well. Such a flexible micro-supercapacitor on paper is promising for future flexible and wearable electronics applications.

Acknowledgements

X. Wang thanks NIMS for the financial support from the internship in NIMS and Dr Tsukagoshi's group for the generous help from the group members. X. Wang thanks Dr Yun Li for insightful discussion about paper based electronics. This work is partly funded by NRF-Create under ''Nanomaterials for energy storage and water management''.

Notes and references

1 X. Xiao, T. Q. Li, P. H. Yang, Y. Gao, H. Y. Jin, W. J. Ni, W. H. Zhan, X. H. Zhang, Y. Z. Cao, J. W. Zhong, L. Gong, W. C. Yen, W. J. Mai, J. Chen, K. F. Huo, Y. L. Chueh, Z. L. Wang and J. Zhou, *ACS Nano*, 2012, **6**, 9200.
2 B. D. Gates, *Science*, 2009, **323**, 1566.
3 S. L. P. Tang, *Trans. Inst. Meas. Control*, 2007, **29**, 283.
4 T. Someya, T. Sekitani, S. Iba, Y. Kato, H. Kawaguchi and T. Sakurai, *Proc. Natl. Acad. Sci. U. S. A.*, 2004, **101**, 9966.
5 K. Takei, T. Takahashi, J. C. Ho, H. Ko, A. G. Gillies, P. W. Leu, R. S. Fearing and A. Javey, *Nat. Mater.*, 2010, **9**, 821.
6 D. Pech, M. Brunet, H. Durou, P. H. Huang, V. Mochalin, Y. Gogotsi, P. L. Taberna and P. Simon, *Nat. Nanotechnol.*, 2010, **5**, 651.
7 M. Beidaghi and C. L. Wang, *Adv. Funct. Mater.*, 2012, **22**, 4501.
8 K. Wang, W. J. Zou, B. G. Quan, A. F. Yu, H. P. Wu, P. Jiang and Z. X. Wei, *Adv. Energy Mater.*, 2011, **1**, 1068.
9 J. J. Yoo, K. Balakrishnan, J. S. Huang, V. Meunier, B. G. Sumpter, A. Srivastava, M. Conway, A. L. M. Reddy, J. Yu, R. Vajtai and P. M. Ajayan, *Nano Lett.*, 2011, **11**, 1423.
10 J. Feng, X. Sun, C. Z. Wu, L. L. Peng, C. W. Lin, S. L. Hu, J. L. Yang and Y. Xie, *J. Am. Chem. Soc.*, 2011, **133**, 17832.
11 J. W. Long, B. Dunn, D. R. Rolison and H. S. White, *Chem. Rev.*, 2004, **104**, 4463.

12 M. Q. Xue, Z. Xie, L. S. Zhang, X. L. Ma, X. L. Wu, Y. G. Guo, W. G. Song, Z. B. Li and T. B. Cao, *Nanoscale*, 2011, **3**, 2703.
13 W. Sun, R. L. Zheng and X. Y. Chen, *J. Power Sources*, 2010, **195**, 7120.
14 Y. Li, C. Liu, Y. Xu, T. Minari, P. Darmawan and K. Tsukagoshi, *Org. Electron.*, 2012, **13**, 815.
15 Y. H. Kim, D. G. Moon and J. I. Han, *IEEE Electron Device Lett.*, 2004, **25**, 702.
16 R. Liu and S. B. Lee, *J. Am. Chem. Soc.*, 2008, **130**, 2942.
17 L. J. Sun, X. X. Liu, K. K. T. Lau, L. Chen and W. M. Gu, *Electrochim. Acta*, 2008, **53**, 3036.
18 Y. Hou, Y. W. Cheng, T. Hobson and J. Liu, *Nano Lett.*, 2010, **10**, 2727.
19 Z. M. Zhang, Z. X. Wei and M. X. Wan, *Macromolecules*, 2002, **35**, 5937.
20 B. C. Beard and P. Spellane, *Chem. Mater.*, 1997, **9**, 1949.
21 K. Zhang, L. L. Zhang, X. S. Zhao and J. S. Wu, *Chem. Mater.*, 2010, **22**, 1392.
22 A. A. Qaiser, M. M. Hyland and D. A. Patterson, *Synth. Met.*, 2012, **162**, 958.
23 M. G. Han and S. S. Im, *Polymer*, 2000, **41**, 3253.
24 M. Chigane and M. Ishikawa, *J. Electrochem. Soc.*, 2000, **147**, 2246.
25 S. Han, J. F. Zhai, L. H. Shi, X. Q. Liu, W. X. Niu, H. J. Li and G. B. Xu, *Electrochem. Commun.*, 2007, **9**, 1434.
26 J. L. Amphlett and G. Denuault, *J. Phys. Chem. B*, 1998, **102**, 9946.
27 F. L. Qiu, N. A. Williams and A. C. Fisher, *Electrochem. Commun.*, 1999, **1**, 124.
28 X. Wang, W. S. Liu, X. H. Lu and P. S. Lee, *J. Mater. Chem.*, 2012, **22**, 23114.
29 E. Frackowiak and F. Beguin, *Carbon*, 2001, **39**, 937.
30 A. G. Pandolfo and A. F. Hollenkamp, *J. Power Sources*, 2006, **157**, 11.
31 M. D. Stoller, S. J. Park, Y. W. Zhu, J. H. An and R. S. Ruoff, *Nano Lett.*, 2008, **8**, 3498.
32 Z. J. Fan, J. Yan, T. Wei, L. J. Zhi, G. Q. Ning, T. Y. Li and F. Wei, *Adv. Funct. Mater.*, 2011, **21**, 2366.
33 P. L. Taberna, P. Simon and J. F. Fauvarque, *J. Electrochem. Soc.*, 2003, **150**, A292.
34 X. Wang, A. Sumboja, M. F. Lin, J. Yan and P. S. Lee, *Nanoscale*, 2012, **4**, 7266.
35 A. Sumboja, C. Y. Foo, J. Yan, C. Y. Yan, R. K. Gupta and P. S. Lee, *J. Mater. Chem.*, 2012, **22**, 23921.
36 Z. J. Fan, J. Yan, T. Wei, L. J. Zhi, G. Q. Ning, T. Y. Li and F. Wei, *Adv. Funct. Mater.*, 2011, **21**, 2366.